Journal of Southeast University (English Edition) Vol. 39, No. 4, pp. 323 - 332 Dec. 2023 ISSN 1003—7985

Damage identification for vertical stiffness of joints of periodic continuous beams based on spectral element method

Zhu Hongping Shen Zehui Weng Shun

(School of Civil and Hydraulic Engineering, Huazhong University of Science and Technology, Wuhan 430074, China)

Abstract: Continuous beam bridges deteriorate during service because of environmental conditions. The stiffness of the supports of the continuous beam degenerates or even fails, severely affecting normal use. To identify the damage to the supports of periodic continuous beams, a damage identification method for vertical stiffness of the joints of periodic continuous beams based on the spectral element method (SEM) is proposed. The beam element adopts an Euler beam, with each cell comprising a beam unit and a joint. The dynamic stiffness matrix of a cell in a beam element is obtained using the SEM. Combined with the joint equilibrium equations, the transfer matrix of a periodic continuous beam can be established. The propagation constant is obtained by solving the eigenvalues of the transfer matrix. An objective function based on the propagation constant is proposed to identify the vertical stiffness damages of the joints of a periodic continuous beam using the interior point method. The proposed method is extensively validated through numerical case studies. Results demonstrate that this method can accurately identify the position and degree of damage to the vertical stiffness of a joint for single- and multi-parameter damage identification.

Key words: joints; periodic continuous beam; wave propagation; spectral element method; propagation constant

DOI: 10.3969/j.issn.1003-7985.2023.04.001

Recently, the structural damage detection of bridges has received considerable attention with the increasing occurrence of bridge safety incidents. The damage identification[1-2] of bridges has always been a popular research topic. Structural damage usually decreases the stiffness within the damaged area, affecting the static or dynamic structural parameters. Traditional structural damage identification uses these parameters to invert the location and extent of structural stiffness reduction. Previous research primarily focused on the frequency and modal shape of bridges for damage identification. The application of natural frequency sensitivity analysis to structural damage identification was first introduced by Cawley and Adams[3], enabling the identification of damage location and severity in simple structures. Wahab and Roeck[4] proposed a damage identification method based on mode shape curvature sensitivity analysis and applied it to practical bridge structures. The traditional structural damage identification method generally adopts the finite element method, which requires the global element stiffness of the structure. Applying this approach to large-scale periodic structures results in high computational effort and inefficiency[5].

Compared with traditional damage identification methods, computational efficiency can be considerably improved by considering the periodic structural properties. The most typical periodic structure is the continuous beam bridge. The continuous supported beam bridge is one of the most widely and highly used bridge types. It has geometric and physical periodicity, particularly with periodically spaced supports (supports are equally spaced and have identical stiffness). For a continuous supported Euler beam, each cell comprises a beam unit and a joint. The adjacent cells are coupled by rotation and shear springs at the joint; therefore, the structure can be considered a double-coupled system. In each cell, the beam can be considered a simply supported beam. The calculation for the beam element is based on the Euler-Bernoulli beam theory. By ignoring the effects of shear deformation and rotational inertia, all transverse displacements are generated by bending. This theory is suitable for continuous beams with a large slenderness ratio. When the boundary conditions of the beam or a bridge are periodic, the simplified model can be considered an ideal periodic continuous beam, and each span of the structure can be considered an identical cell. Periodic structures require only low-dimensional matrix computations, which can considerably improve the computational efficiency compared to the traditional finite element method that requires high-dimensional matrix computations. The efficiency improvement will be more obvious for large-scale engineering. A beam or bridge exhibiting physical and material periodicity is highly suitable for this method.

Several similar periodic structures exist, and the dynamic characteristics of periodic structures have been extensively studied[6-32]. The essential characteristic of peri-

Received 2023-08-17, **Revised** 2023-10-30.

Biography: Zhu Hongping (1965—), male, doctor, professor, hpzhu@hust.edu.cn.

Foundation item: The National Natural Science Foundation of China (No. 52078233, 51838006).

Citation: Zhu Hongping, Shen Zehui, Weng Shun. Damage identification for vertical stiffness of joints of periodic continuous beams based on spectral element method[J]. Journal of Southeast University (English Edition), 2023, 39(4): 323 - 332. DOI: 10.3969/j.issn.1003-7985.2023.04.001.

odic structures is the presence of frequency pass bands and stop bands. When elastic waves or disturbances have frequencies within the pass band region of the structure, the waves or disturbances propagate throughout the structure without limitations, and their amplitude and energy do not decay. Conversely, when the frequency of elastic waves or disturbances is in the stop band region of the structure, the amplitude and energy of the waves do not propagate throughout the structure but will attenuate. Band gaps can be described by the propagation constant. When the real part of the propagation constant is equal to 0, it represents the pass band. Otherwise, the band represents the stop band. Potentially, an objective function based on band gap characteristics can be established for damage identification. The calculation method of elastic wave band gaps is the basis for studying the wave propagation characteristics of periodic structures. At present, the transfer matrix[30-32], plane wave expansion[19], finite-difference time-domain, multiple-scattering, and finite element methods are typically used to calculate the band gaps of periodic structures.

The transfer matrix method was first applied to the flexural wave characteristics of the periodic support pipe beam system by Koo and Park[32], and the presence of flexural vibration band gaps was experimentally verified. When the excitation frequency range of the load is determined, a reasonable design of the position of periodic support can effectively reduce the vibration propagation of the structure. The transfer matrix method used to analyze wave propagation in periodic structures can considerably enhance computational efficiency. However, boundary condition damages may substantially affect the band gap characteristics of periodic structures, possibly leading to a modal localization phenomenon[34-36]. The modal localization phenomenon is manifested as the modal jump occurs and energy accumulates at the locations where damage to the beam occurs[34]. Although the principle of wave propagation of periodic continuous beams has been extensively studied, identifying the damages of periodic structures, particularly the boundary conditions, remains challenging.

The spectral element method (SEM) is used to analyze wave propagation. This approach is advantageous in at least two aspects. In the SEM, the displacement function can be expressed as the general solution of the wave equation, and the dynamic stiffness matrix can be obtained in the frequency domain. The SEM provides high accuracy, particularly when addressing problems involving irregular geometries or complex boundary conditions. In addition, it can achieve exponential convergence rates for smooth solutions. For periodic structures, each cell is represented by the same dynamic stiffness matrix, rendering the SEM computation efficient and thus allowing for its wide application. Considering a beam as an example, when analyzing wave propagation, the mesh size of the finite element method depends on the wavelength, which may require tens of thousands of element nodes, whereas the frequency domain spectral element rule only requires one element and two nodes. This feature can considerably improve computational efficiency, particularly for periodic continuous structures.

In this study, the boundary conditions of the joints of a continuous beam are the research focus. The boundary conditions of the joints include the vertical and rotational stiffness. Among these boundary conditions, this study mainly focuses on the vertical stiffness of the support. The objective function is established based on the propagation constant. The dynamic stiffness matrix of an Euler beam in one cell is established using the SEM, and the equilibrium equation of the joints is obtained using the boundary continuity condition. Combined with the dynamic stiffness matrix and the equilibrium equation of the joints, the transfer matrix can be obtained. The propagation constant can be calculated by solving the eigenvalues of the transfer matrix. An objective function based on the propagation constant is proposed to identify the vertical stiffness damages of the joints of periodic continuous beams. The position and width of the wave propagation band gap determined by the propagation constant are validated by analyzing the transfer properties and deformations of periodic beams. The proposed method is extensively evaluated through numerical case studies. The results demonstrate that this method can accurately identify the position and degree of damage of the vertical stiffness of a joint for single- and multi-parameter damage cases.

1 Transfer Matrix Method Based on the Spectral Element Method

1.1 Equation of the wave motion transfer matrix

Continuous beam bridges can be simplified as equivalent multi-supported beams in dynamic analysis. If the supports are equally spaced and have equal stiffness and damping, the beam is referred to as a periodic supported beam. As shown in Fig. 1, a periodic simply supported Bernoulli-Euler beam comprises a few repetitively arranged subcells.

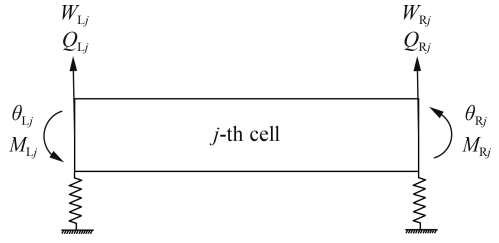

Fig. 1 j-th cell of a simply supported Bernoulli-Euler beam

Herein, for low-frequency bending vibrations, the shearing deformation and rotational inertia are relatively

small and can be neglected. By adopting Bernoulli-Euler beam theory, the differential equation of wave motion for the beam of the j-th cell can be derived as

$$EI\frac{\partial w_j^4}{\partial x^4}+\rho A\frac{\partial w_j^2}{\partial t^2}=0 \tag{1}$$

where $w(x, t)$ represents the transverse displacement; E represents Young's modulus; A and I represent the cross-sectional area and area moment of inertia about the neutral axis, respectively; ρ represents the mass density.

The spectral form of the solution to Eq. (1) is assumed to be

$$w(x, t) = \frac{1}{N}\sum_{n=0}^{N-1} W_n(x; w_n)\,\mathrm{e}^{\mathrm{i}\omega t} \tag{2}$$

Substituting Eq. (2) into Eq. (1) gives an eigenvalue problem for a specific discrete frequency (such as $\omega=\omega_n$) as follows:

$$EI\frac{\partial W}{\partial x^4}-\omega^2\rho AW=0 \tag{3}$$

The general solution to Eq. (3) has the form as

$$W(x) = a\mathrm{e}^{-\mathrm{i}k(\omega)x} \tag{4}$$

Substituting Eq. (4) into Eq. (3) as

$$k^4-k_{\mathrm{F}}^4=0 \tag{5}$$

where k_{F} represents the wavenumber for pure bending, which is defined as

$$k_{\mathrm{F}}=\sqrt{\omega}\left(\frac{\rho A}{EI}\right)^{1/4} \tag{6}$$

Eq. (5) gives four roots, including two real roots and two pure imaginary roots,

$$k_1=-k_2=k_{\mathrm{F}},\quad k_3=-k_4=\mathrm{i}k_{\mathrm{F}} \tag{7}$$

The general solution Eq. (3) can be then obtained as

$$w(x, \omega) = a_1\mathrm{e}^{-\mathrm{i}k_{\mathrm{F}}x}+a_2\mathrm{e}^{-k_{\mathrm{F}}x}+a_3\mathrm{e}^{+\mathrm{i}k_{\mathrm{F}}x}+a_4\mathrm{e}^{k_{\mathrm{F}}x} \tag{8}$$

where a_n (n = 1, 2, 3, 4) represent the constants determined by boundary conditions.

In the j-th cell, the vertical displacement and angular boundary conditions at both ends of the Euler beam can be expressed as

$$W_{\mathrm{L}j}=W_j(0),\ \theta_{\mathrm{L}j}=\theta_j(0),\ W_{\mathrm{R}j}=W_j(l_j),\ \theta_{\mathrm{R}j}=\theta_j(l_j) \tag{9}$$

The spectral nodal displacements and slopes of the j-th cell (see Fig. 2) can be related to the displacement field by substituting Eq. (8) into the right-hand side of Eq. (9), yielding the relation between the displacement vector d and the coefficient vector $\boldsymbol{a}$ as

$$\boldsymbol{d}=\boldsymbol{H}_1\boldsymbol{a} \tag{10}$$

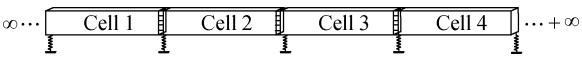

Fig. 2 Simply supported Bernoulli-Euler beam

where

$$\boldsymbol{H}_1=\begin{bmatrix}1 & 1 & 1 & 1\\ -\mathrm{i}k_{\mathrm{F}} & -k_{\mathrm{F}} & \mathrm{i}k_{\mathrm{F}} & k_{\mathrm{F}}\\ \mathrm{e}^{-\mathrm{i}k_{\mathrm{F}}L} & \mathrm{e}^{-k_{\mathrm{F}}L} & \mathrm{e}^{\mathrm{i}k_{\mathrm{F}}L} & \mathrm{e}^{k_{\mathrm{F}}L}\\ -\mathrm{i}k_{\mathrm{F}}\mathrm{e}^{-\mathrm{i}k_{\mathrm{F}}L} & -k_{\mathrm{F}}\mathrm{e}^{-k_{\mathrm{F}}L} & \mathrm{i}k_{\mathrm{F}}\mathrm{e}^{\mathrm{i}k_{\mathrm{F}}L} & k_{\mathrm{F}}\mathrm{e}^{-k_{\mathrm{F}}L}\end{bmatrix} \tag{11}$$

$$\boldsymbol{a}=\{a_1, a_2, a_3, a_4\}^{\mathrm{T}}$$
$$\boldsymbol{d}=\{W_{\mathrm{L}j}, \theta_{\mathrm{L}j}, W_{\mathrm{R}j}, \theta_{\mathrm{R}j}\}$$

The shear forces and bending moments at both ends of the j-th cell can be expressed as

$$Q_{\mathrm{L}j}=-EI\frac{\partial W_j(0)}{\partial x^3},\quad M_{\mathrm{L}j}=EI\frac{\partial W_j(0)}{\partial x^2} \tag{12}$$

$$Q_{\mathrm{R}j}=-EI\frac{\partial W_j(l_j)}{\partial x^3},\quad M_{\mathrm{R}j}=EI\frac{\partial W_j(l_j)}{\partial x^2} \tag{13}$$

Substituting Eq. (8) into Eq. (13) yields the relation between the force vector $\boldsymbol{F}_j$ and the coefficient vector $\boldsymbol{a}$ as follows:

$$\boldsymbol{F}_j=\boldsymbol{G}\boldsymbol{a} \tag{14}$$

where

$$\boldsymbol{F}_j=\{Q_{\mathrm{L}j},\ M_{\mathrm{L}j},\ Q_{\mathrm{R}j},\ M_{\mathrm{R}j}\}$$

$$\boldsymbol{G}=\begin{bmatrix}-\mathrm{i}k_{\mathrm{F}}^3 & -k_{\mathrm{F}}^3 & \mathrm{i}k_{\mathrm{F}}^3 & k_{\mathrm{F}}^3\\ k_{\mathrm{F}}^2 & k_{\mathrm{F}}^2 & -k_{\mathrm{F}}^2 & k_{\mathrm{F}}^2\\ -\mathrm{i}k_{\mathrm{F}}^3\mathrm{e}^{-\mathrm{i}k_{\mathrm{F}}L} & -k_{\mathrm{F}}^3\mathrm{e}^{-k_{\mathrm{F}}L} & \mathrm{i}k_{\mathrm{F}}^3\mathrm{e}^{\mathrm{i}k_{\mathrm{F}}L} & k_{\mathrm{F}}^3\mathrm{e}^{k_{\mathrm{F}}L}\\ k_{\mathrm{F}}^2\mathrm{e}^{-\mathrm{i}k_{\mathrm{F}}L} & k_{\mathrm{F}}^2\mathrm{e}^{-k_{\mathrm{F}}L} & -k_{\mathrm{F}}^2\mathrm{e}^{\mathrm{i}k_{\mathrm{F}}L} & k_{\mathrm{F}}^2\mathrm{e}^{k_{\mathrm{F}}L}\end{bmatrix}$$

The coefficient vector $\boldsymbol{a}$ can be eliminated from Eq. (10) and Eq. (14) to obtain the relation between the force vector $\boldsymbol{F}_j$ and the nodal DOF vector $\boldsymbol{d}$ as follows:

$$\boldsymbol{F}_j=\boldsymbol{K}_j^{\mathrm{B}}\boldsymbol{d} \tag{15}$$

where

$$\boldsymbol{K}_j^{\mathrm{B}}=\boldsymbol{G}(\boldsymbol{H}_1)^{-1} \tag{16}$$

where $\boldsymbol{K}_j^{\mathrm{B}}$ represents the dynamic stiffness matrix for the flexural vibration of the j-th cell,

$$\boldsymbol{K}_j^{\mathrm{B}}=\begin{bmatrix}K_{j11}^{\mathrm{B}} & K_{j12}^{\mathrm{B}} & K_{j13}^{\mathrm{B}} & K_{j14}^{\mathrm{B}}\\ K_{j21}^{\mathrm{B}} & K_{j22}^{\mathrm{B}} & K_{j23}^{\mathrm{B}} & K_{j24}^{\mathrm{B}}\\ K_{j31}^{\mathrm{B}} & K_{j32}^{\mathrm{B}} & K_{j33}^{\mathrm{B}} & K_{j34}^{\mathrm{B}}\\ K_{j41}^{\mathrm{B}} & K_{j42}^{\mathrm{B}} & K_{j43}^{\mathrm{B}} & K_{j44}^{\mathrm{B}}\end{bmatrix} \tag{17}$$

1.2 Joint equilibrium equation of the transfer matrix

The dynamics of the Bernoulli-Euler beam in the j-th cell are represented in terms of the dynamic stiffness block matrix,

$$\begin{bmatrix} \boldsymbol{K}_{\mathrm{LL}j} & \boldsymbol{K}_{\mathrm{LR}j} \\ \boldsymbol{K}_{\mathrm{RL}j} & \boldsymbol{K}_{\mathrm{RR}j} \end{bmatrix} \begin{bmatrix} \boldsymbol{d}_{\mathrm{L}j} \\ \boldsymbol{d}_{\mathrm{R}j} \end{bmatrix} = \begin{bmatrix} \boldsymbol{F}_{\mathrm{L}j} \\ \boldsymbol{F}_{\mathrm{R}j} \end{bmatrix} \tag{18}$$

where $\boldsymbol{K}_{grj}$ (g, r = L, R) represents the two-by-two partitioned submatrices of $\boldsymbol{K}_j^{\mathrm{B}}$.

Eq. (18) can be transformed to relate the state vectors at two ends of the j-th cell,

$$\begin{bmatrix} \boldsymbol{d}_{\mathrm{R}j} \\ \boldsymbol{F}_{\mathrm{R}j} \end{bmatrix} = \begin{bmatrix} -\boldsymbol{K}_{\mathrm{LR}j}^{-1}\boldsymbol{K}_{\mathrm{LL}j} & \boldsymbol{K}_{\mathrm{LR}j}^{-1} \\ \boldsymbol{K}_{\mathrm{RL}j}-\boldsymbol{K}_{\mathrm{RR}j}\boldsymbol{K}_{\mathrm{LR}j}^{-1}\boldsymbol{K}_{\mathrm{LL}j} & \boldsymbol{K}_{\mathrm{RR}j}\boldsymbol{K}_{\mathrm{LR}j}^{-1} \end{bmatrix} \begin{bmatrix} \boldsymbol{d}_{\mathrm{L}j} \\ \boldsymbol{F}_{\mathrm{L}j} \end{bmatrix} \tag{19}$$

Eq. (19) can be rewritten as

$$\boldsymbol{Y}_{\mathrm{R}j} = \boldsymbol{T}_{js}\boldsymbol{Y}_{\mathrm{L}j} \tag{20}$$

where $\boldsymbol{Y}_{\mathrm{R}j} = [\,\boldsymbol{d}_{\mathrm{R}j} \quad \boldsymbol{F}_{\mathrm{R}j}\,]$ and $\boldsymbol{Y}_{\mathrm{L}j} = [\,\boldsymbol{d}_{\mathrm{L}j} \quad \boldsymbol{F}_{\mathrm{L}j}\,]$ represent the state vectors at the left and right ends of j-th cell of the Bernoulli-Euler beam, respectively.

Considering the wave propagation between the j-th and $(j+1)$-th cells, the joint equilibrium equation in the frequency domain can be expressed as

$$\begin{Bmatrix} Q_{\mathrm{R}j} \\ M_{\mathrm{R}j} \\ Q_{\mathrm{L}(j+1)} \\ M_{\mathrm{L}(j+1)} \end{Bmatrix} = \begin{bmatrix} k_{\mathrm{w}} & 0 & -k_{\mathrm{w}} & 0 \\ 0 & 0 & 0 & -k_{\theta} \\ -k_{\mathrm{w}} & 0 & k_{\mathrm{w}} & 0 \\ 0 & -k_{\theta} & 0 & k_{\theta} \end{bmatrix} \begin{Bmatrix} W_{\mathrm{R}j} \\ \theta_{\mathrm{R}j} \\ W_{\mathrm{L}(j+1)} \\ \theta_{\mathrm{L}(j+1)} \end{Bmatrix} \tag{21}$$

where k_{w} and k_{θ} represent vertical and rotational stiffness of the j-th joint, respectively.

Eq. (19) can be further rewritten as

$$\begin{Bmatrix} W_{\mathrm{L}(j+1)} \\ \theta_{\mathrm{L}(j+1)} \\ Q_{\mathrm{L}(j+1)} \\ M_{\mathrm{L}(j+1)} \end{Bmatrix} = \begin{bmatrix} 1 & 0 & -k_{\mathrm{w}}^{-1} & 0 \\ 0 & 1 & 0 & -k_{\theta}^{-1} \\ 0 & 0 & -1 & 0 \\ 0 & 0 & 0 & -1 \end{bmatrix} \begin{Bmatrix} W_{\mathrm{R}j} \\ \theta_{\mathrm{R}j} \\ Q_{\mathrm{R}j} \\ M_{\mathrm{R}j} \end{Bmatrix} \tag{22}$$

Eq. (19) can be simplified as

$$\boldsymbol{Y}_{\mathrm{L}(j+1)} = \boldsymbol{T}_{jj}\boldsymbol{Y}_{\mathrm{R}j} \tag{23}$$

Substituting Eq. (23) into Eq. (20), the relation between the state vectors of the j-th and $(j+1)$-th cells can obtained as

$$\boldsymbol{Y}_{\mathrm{L}(j+1)} = \boldsymbol{T}_{jj}\boldsymbol{Y}_{\mathrm{R}j} = \boldsymbol{T}_{jj}\boldsymbol{T}_{js}\boldsymbol{Y}_{\mathrm{L}j} = \boldsymbol{T}_{j}\boldsymbol{Y}_{\mathrm{L}j} \tag{24}$$

where

$$\boldsymbol{T}_{j} = \boldsymbol{T}_{jj}\boldsymbol{T}_{js} \tag{25}$$

where $\boldsymbol{T}_j$ represents the transfer matrix between two adjacent cells.

1.3 Propagation constant

For harmonic periodic structures, the transfer matrix between all adjacent cells remains the same.

Eq. (24) can be simplified as

$$\boldsymbol{Y}_{j+1} = \boldsymbol{T}_{j}\boldsymbol{Y}_{j} \tag{26}$$

The wave propagation in the infinite periodic structure is governed by the eigenvalues of the transfer matrix $\boldsymbol{T}$. Therefore, Eq. (26) can be given as

$$\boldsymbol{Y}_{j+1} = c_n\boldsymbol{Y}_{j} \tag{27}$$

where c_n represents the eigenvalue of the transfer matrix $\boldsymbol{T}$. These eigenvalues are in pairs, with a pair representing the same wave but in opposite directions. Therefore, c_n defines the relation between the state vectors at two adjacent cells of the infinite periodic structure. The propagation constant c_n can be given as

$$c_n = \mathrm{e}^{\mu_n} = \mathrm{e}^{\gamma_n + \mathrm{i}\beta_n} \tag{28}$$

The amplitude decay of wave propagation between the adjacent cells and β_n, which is called the phase shift constant, denotes the phase difference between adjacent cells. According to the definition of the propagation constant, the real and imaginary parts represent the attenuation and phase constants, respectively. When $\gamma_n = 0$, the wave can propagate without attenuation, and the phase changes when crossing every cell; meanwhile, the corresponding frequency region is called the pass band. In contrast, when $\gamma_n \neq 0$, the wave will decay and can be identified by analyzing the real parts of the propagation constants, and the corresponding frequency region is called the stop band. Among these pairs of propagation constants, only a pair with the least attenuation is focused on in this paper because it represents the most dominant form of attenuation. The frequency band characteristics of the infinite periodic structure are analyzed using the propagation constant to study the law of wave propagation.

2 Damage Identification Based on the Propagation Constant

2.1 Determining the occurrence of damage

For a finite periodic simply supported Bernoulli-Euler beam, the transfer matrix and the joint equilibrium equation remain the same, and the transfer matrix $\boldsymbol{T}$ for the entire beam comprising n cells can be expressed as follows:

$$\boldsymbol{T} = \boldsymbol{T}_1\boldsymbol{T}_2\cdots\boldsymbol{T}_{j-1}\boldsymbol{T}_j\cdots\boldsymbol{T}_n \tag{29}$$

If no damage occurs, $\boldsymbol{T}_i$ ($i = 1, 2, \ldots, n$) is unchanged.

According to the derivation process in Section 1.3, the propagation constant for the beam can be gained from Eqs. (26) to (28) as follows:

$$\mu = \ln c_n \tag{30}$$

If no damage occurs, the original propagation constant μ will not change for a periodic structure with a certain parameter N. If damage occurs, the beam transfer matrix

$\boldsymbol{T}$ will change, and the propagation constant μ_d will change accordingly. Comparing μ and μ_d can determine whether damage has occurred.

2.2 Objective function based on the propagation constant

This section combines the transfer matrix method with the SEM, which is more efficient for calculating the frequency domain characteristics of periodic structures and more effective at identifying the position and degree of damage of the joint. As mentioned above, the main focus of this paper is on the damage to the joint. Assume that the dynamic stiffness matrix for the beam $\boldsymbol{T}_{js}$ remains the same. The joint equilibrium equation $\boldsymbol{T}_{jj}$ involves the variables k_{w} and k_θ. The rotation of the structure is primarily controlled by the beam unit and is minimally influenced by the rotation stiffness of the joint. Therefore, k_{w} is the key discussed in this paper.

Assuming the periodic structure has 10 cells, the steps for damage identification of variable k_{w} are as follows:

1) Establish the dynamic stiffness matrix of beam cells based on the SEM.

2) Based on the boundary conditions, obtain the equilibrium equation of the joint between the two cells.

3) If the periodic structure is undamaged, the transfer matrix can be expressed as

$$\boldsymbol{T} = \boldsymbol{T}_1^{10} \tag{31}$$

When the periodic structure is damaged, the transfer matrix where the damage occurred is changed. Assume that the undamaged vertical stiffness of the joint in the j-th element is expressed as $k_{\mathrm{w}j}(j = 1, 2, \ldots, 10)$. Similarly, assume that the stiffness factor of the vertical stiffness of the j-th joint is expressed as $\theta_j(j = 1, 2, \ldots, 10)$; for example, the damaged equilibrium equation of the first joint can be expressed as

$$\boldsymbol{T}_1 = \boldsymbol{T}_{jj}\boldsymbol{T}_{js} = \begin{bmatrix} 1 & 0 & -\theta_1 k_{\mathrm{w}1}^{-1} & 0 \\ 0 & 1 & 0 & -k_\theta^{-1} \\ 0 & 0 & -1 & 0 \\ 0 & 0 & 0 & -1 \end{bmatrix} \boldsymbol{T}_{1s} \tag{32}$$

and the transfer matrix of the entire structure can be expressed as a multiplication of every transfer matrix of 10 cells,

$$\boldsymbol{T} = \boldsymbol{T}_1\boldsymbol{T}_2\boldsymbol{T}_3\boldsymbol{T}_4\boldsymbol{T}_5\boldsymbol{T}_6\boldsymbol{T}_7\boldsymbol{T}_8\boldsymbol{T}_9\boldsymbol{T}_{10} \tag{33}$$

4) Calculate and compare the propagation constants of the undamaged and damaged states. The presence of damage is proved by a substantial difference between the two propagation constants.

5) The structural parameters that should be identified are the stiffness factors of the vertical stiffness of the joints $\theta_j(j = 1, 2, \ldots, 10)$. The unknown substructural parameter θ_j can be estimated by minimizing the discrepancy between the original and damaged states, and the objective function for iteration is shown as

$$f_{\mathrm{obj}} = \sum_{\omega=1}^{n} (\gamma_0 - \gamma_{\mathrm{d}})^2 \tag{34}$$

where γ_0 and γ_{d} are the real parts of the propagation constant in the original undamaged state and the damaged state, respectively. Every frequency has a corresponding value of the real part of the propagation constant.

6) The algorithm adopts the interior point method for solving linear programming or nonlinear convex optimization problems. The iteration of the objective function continues until

$$f_{\mathrm{obj},n} \leqslant \xi, \quad \frac{|f_{\mathrm{obj},n+1} - f_{\mathrm{obj},n}|}{f_{\mathrm{obj},n}} \leqslant \varepsilon, \quad n \leqslant N_{\max} \tag{35}$$

where n is the number of iterations; ξ is the allowable error; ε is the allowable residual; $N_{\max}$ is the maximum number of iterations.

7) For every parameter θ, there is a real part of propagation constant γ. The most commonly used update method is the sensitivity-based update. Assuming m frequencies are taken in the range of 0 to 1 000 Hz, the vector $\boldsymbol{g}$ can be expressed as

$$\boldsymbol{g}(\theta) = \{\gamma_1, \gamma_2, \ldots, \gamma_m\}^{\mathrm{T}} \tag{36}$$

The model update process involves minimizing the weighted residual $\boldsymbol{g}(\theta)$, aiming to ideally reduce it to zero. However, because of errors in the model and the damaged model, it can only be minimized. Because the real parts of propagation constants depend nonlinearly on the update parameters, a linear approximation must be used,

$$\boldsymbol{g}(\theta) = g(0) + \bar{\boldsymbol{S}}\theta \tag{37}$$

where $\bar{\boldsymbol{S}}$ denotes the sensitivity matrix or Jacobian. The residual is then

$$\boldsymbol{r}(\theta) = r_0 - \boldsymbol{S}\theta \tag{38}$$

where $r_0 = g^{\mathrm{dama}} - g(0)$ is the difference between the damaged values and the values from the undamaged model; $\boldsymbol{S}$ is the sensitivity matrix, which can be obtained using the finite-difference method.

$$\boldsymbol{S} = \frac{\partial g(\theta)}{\partial \theta} \qquad \theta = 0 \tag{39}$$

The update can be performed by minimizing the linearized residual as follows:

$$\min \| \boldsymbol{S}\theta - r_0 \|_2^2 \tag{40}$$

Setting the derivative with respect to an equal to zero leads to the well-known least-squares solution as follows:

$$\theta = (\boldsymbol{S}^{\mathrm{T}}\boldsymbol{S})^{-1}\boldsymbol{S}^{\mathrm{T}}r_0 \tag{41}$$

3 Numerical Case Studies

In this section, the effects of various parameters on the wave propagation characteristics of a periodic simply supported Euler-Bernoulli beam and various detuning states are studied in terms of the vertical stiffness of the joint. The numerical predictions are validated by evaluating the transfer property and the deformation of the periodic simply supported beam through a finite element analysis. The material properties and geometric parameters used in the numerical analysis are listed in Table 1.

Table 1 Geometric and material properties in the analysis

Description	Value
Length of the beam L/m	7
Number of spans N	10
Dimensionless vertical stiffness of the joint k_w/(N · m^{-1})	3.4
Dimensionless rotational stiffness of the joint k_θ/(N · m · rad^{-1})	$+\infty$
Moment of inertia I/m^4	1.637
Mass density ρ/(kg · m^{-3})	2 500
Young's modulus E/(N · m^{-2})	34.4
Transverse cross-sectional area A/m^2	2.8

3.1 Propagation constants for the ordered periodic supported beam

According to the method in Section 3, the propagation constants can be obtained using Eqs. (26) to (28). The transfer matrix $\boldsymbol{T}$ can be obtained according to the structures of the numerical case, and then the eigenvalues c_n of matrix $\boldsymbol{T}$ can be gained by solving the characteristic equation. The propagation constants μ_n are the logarithm of c_n. The real part of μ_n is the attenuation constant γ_n, used to consider the influence of different parameters on the propagation and localization characteristics of the periodic supported beam model.

Fig. 3 shows the effects of the vertical stiffness of the joint between adjacent cells for flexural vibration. As the vertical stiffness of the cell joint increases from 0.034 to 3.4 GN/m, the number of stop bands in a specific frequency range remains constant. The width of the stop bands consistently begins to increase. In every frequency stop band, the lower limit of the range remains constant while the upper limit continuously increases. For a specific vertical stiffness of the cell joint, the width and the upper limit of the range of stop bands continuously increase at high frequencies. For different vertical stiffnesses, it is relatively small when $k_w = 34$ MN/m, and the amplitude increases very slowly compared to the case when $k_w = 3.4$ GN/m. In the first band gap, the peak value at $k_w = 3.4$ GN/m is 0.848, over 16-fold larger than the corresponding peak value of 0.051 at $k_w = 34$ MN/m. Nevertheless, the peak value at $k_w = 3.4$ GN/m gradually increases with frequency, ranging from 0.848 to 0.880, whereas the peak value at $k_w = 34$ MN/m undergoes rapid escalation, soaring from 0.051 to 0.794.

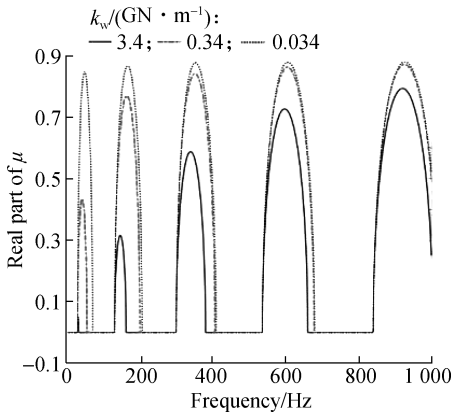

Fig. 3 Real part of the propagation constant versus frequency for different vertical stiffnesses of the joint of a cell

Clearly, altering the vertical stiffness of the joint changes the width of the stop bands of flexural waves.

3.2 Transfer property and deformation of the periodic beam

The results of the previous section can be verified by evaluating the transfer characteristics of a finite number of periodic supported beam cells, where the external force is located at one end of the periodic beam, thus generating a transverse displacement of the cell, and the response at the other end is evaluated using the transfer matrix method. The transfer matrix is obtained using Eq. (25). For example, the total transfer matrix for the ten periodic cells is $\boldsymbol{T} = \prod_{j=1}^{10} \boldsymbol{T}_j$, and the state vectors at the two ends are $\boldsymbol{Y}_{\mathrm{L1}} = \{1,\ \bar{\theta}_{\mathrm{L1}},\ Q_{\mathrm{L1}},\ 0\}^{\mathrm{T}}$ and $\boldsymbol{Y}_{\mathrm{R10}} = \{\bar{w}_{\mathrm{R10}},\ \bar{\theta}_{\mathrm{R10}},\ 0,\ 0\}^{\mathrm{T}}$.

The relation between the state vectors can be represented as

$$\begin{bmatrix} \bar{w}_{\mathrm{R10}} \\ \bar{\theta}_{\mathrm{R10}} \\ 0 \\ 0 \end{bmatrix} = \begin{bmatrix} T'_{11} & T'_{12} & T'_{13} & T'_{14} \\ T'_{21} & T'_{22} & T'_{23} & T'_{24} \\ T'_{31} & T'_{32} & T'_{33} & T'_{34} \\ T'_{41} & T'_{42} & T'_{43} & T'_{44} \end{bmatrix} \begin{bmatrix} 1 \\ \bar{\theta}_{\mathrm{L1}} \\ Q_{\mathrm{L1}} \\ 0 \end{bmatrix} \tag{42}$$

where $T_{ab}(a, b = 1, 2, 3, 4)$ are the components of $\boldsymbol{T}'$. The transverse displacement at the other end can be obtained using Eq. (36).

Fig. 4 shows the transfer property of the ordered periodic beam with 10 cells. Two localization drop curves are within the frequency range of 0 to 200 Hz in Fig. 4, in which the frequency ranges of the first two drops are $f \in (33.582, 35.969)$ Hz and $f \in (134.486, 165.680)$ Hz. The wave cannot propagate within these frequency ranges. The locations and widths of the frequency stop bands agree with the predictions based on the propagation con-

stants shown in Fig. 3.

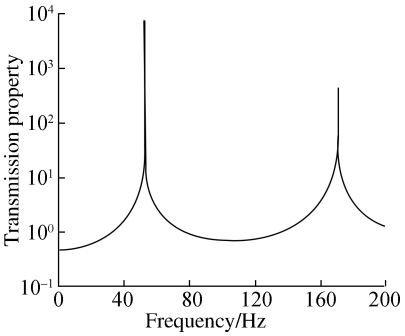

Fig. 4 Transfer property of the ordered periodic beam with 10 cells

3.3 Damage identification

If the vertical stiffness of every cell joint is expressed as one parameter, θ_j, then $\theta_1 = \theta_2 = \ldots = \theta_{10}$, the damage identification can be solved in one cell by only modifying one parameter, and every stiffness coefficient of the vertical stiffness is reduced simultaneously. Five damage scenarios are considered in this paper, and the detailed damage configurations are shown in Table 2.

Table 2 Numerical simulation cases for the 10-cell periodic beam

Case No.	Case description
1	$\theta_i = 1 (i = 1, 2, \ldots, 10)$
2	$\theta_i = 0.5 (i = 1, 2, \ldots, 10)$
3	$\theta_1 = 0.7, \theta_i = 1 (i = 2, 3, \ldots, 10)$
4	$\theta_5 = 0.7, \theta_i = 1 (i = 1, 2, 3, 4, 6, 7, 8, 9, 10)$
5	$\theta_2 = \theta_9 = 0.5, \theta_i = 1 (i = 1, 3, 4, 5, 6, 7, 8, 10)$
6	$\theta_1 = \theta_5 = 0.5, \theta_6 = 0.7, \theta_i = 1 (i = 2, 3, 4, 7, 8, 9, 10)$

For Case 1, $\theta_i = 1 (i = 1, 2, \ldots, 10)$, representing a healthy, damage-free structure. For Case 2, $\theta_i = 0.5 (i = 1, 2, \ldots, 10)$, representing simultaneous damage to the same degree to every cell of the structure, which means that only one variable needs to be modified for the entire structure. For Case 3 and Case 4, only one parameter is to be set for damage identification, and damage occurs in the 1st and 5th cells, representing the different conditions of side span and mid-span damage, respectively. For Case 5 and Case 6, more than one instance of damage occurs in the structure: In Case 5, the 2nd and 9th cells are damaged to the same degree; and in Case 6, the 1st, 5th, and 6th cells of the structure are damaged to simulate a multiple damage condition.

3.3.1 Single-parameter damage identification

When the damage of each cell is identical, i.e., $\theta_i = a$ $(i = 1, 2, \ldots, 10)$, where a is a constant, then it becomes a single-parameter damage identification problem. Considering Case 2 as an example, a is equal to 0.5, and it is clear that θ_i is the parameter to be modified. Eq. (34) shows that the objective function f_{obj} is related to the frequency. For a certain frequency, the real part of the propagation constant of the undamaged and damaged conditions are γ_0 and γ_d, respectively, and the objective function is expressed as the sum of the squares of the difference between γ_0 and γ_d for a certain frequency range. The initial value of the vertical stiffness coefficient θ_i is 1.0, and the convergence condition of the objective function is shown in Eq. (35). The values of the allowable error ξ and the allowable residual ε are 1×10^{-16}. Fig. 5 clearly shows that the uncertain scaling parameters eventually converge to constant values, indicating that the stiffness coefficient of the vertical stiffness is 0.5 after three iterative estimations. The figure shows that the single-parameter damage identification considerably quickly converges.

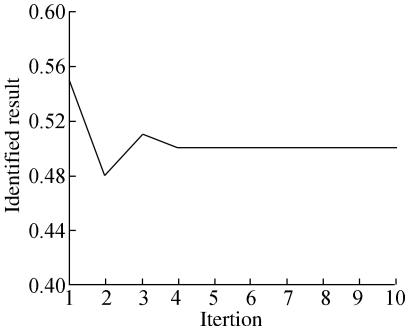

Fig. 5 History of iterative simultaneous estimation of the vertical stiffness coefficient for Case 2

3.3.2 Multi-parameter damage identification

In this section, the most complex situation of the numerical study is considered: Each vertical stiffness coefficient of each cell $\theta_i (i = 1, 2, \ldots, 10)$ is a parameter to be modified.

The damage identification process can be summarized as follows: 1) calculate the transfer matrix for the entire structure; 2) calculate the propagation constant for the transfer matrix; 3) follow the process in Section 2.2 to obtain the objective function f_{obj} about θ_i; 4) obtain the target-identified value based on the objective function.

Case 3 is considered as an example. It simulates the damage occurring at the side span. The vertical stiffness coefficient of the joint of the first cell is reduced to 0.5, and other cells are healthy. This result illustrates that the damage of the single support occurs in this case. Similarly, in Case 4, the damage occurs in the fifth cell of the structure.

The 10-cell periodic beam is a symmetrical structure (see Fig. 6), and damage at a symmetric location produces a very similar effect for wave propagation such that the propagation constant exhibits similar properties. The vertical stiffness coefficient of the joint to be modified has a similar situation. In Fig. 6, the damaged cell is the first cell, but the identification result reveals that the last cell is the damaged cell.

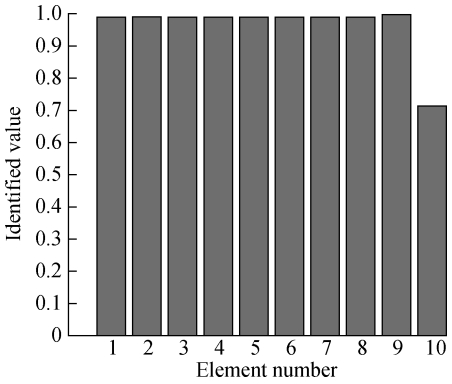

Fig. 6 Identified results of iterations for Case 3 in the numerical study

Fig. 7 shows that the 10-cell periodic beam is a symmetrical structure. In Case 4, the damaged cell is the 5th cell. This case simulates damage occurring near the midspan. Fig. 7 shows the identified value plotted against the element number. The identified value of the 5th cell is about 0.7, and those for others are in the range of 0.9 to 1.0, with the exception of the identified value of element 10, which is about 0.94, and the identified values of other elements are close to 1.0. The numerical case proves the accuracy of multi-parameter damage identification.

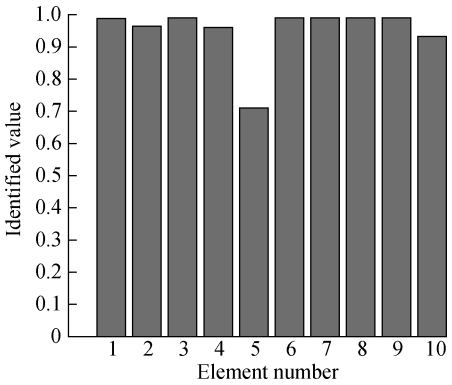

Fig. 7 Identified results of iterations for Case 4 in the numerical study

Damage is often unpredictable in practical engineering. The location and degree of damage are random. Therefore, it is meaningful to simultaneously identify the degree and location of multiple damages to the structure.

In this section, Case 5 simulates the damages to the 2nd and 9th cells, and Case 6 simulates the damage to the 1st, 5th, and 6th cells. The damage identification process is similar to the previous cases. In Fig. 8, the identified values of the 2nd and 9th cells are about 0.5, which is very close to the true value. For the other healthy cells, the identified value oscillates, ranging from 0.9 to 1.0, but the identified value of the 7th and 8th cells ranges from 0.9 to 0.95, which is smaller than that of other healthy cells. In Fig. 9, the identified value is about 0.5 for the 1st and 5th cells and 0.6 for the 6th cell; meanwhile, the identified value of other healthy cells is very near to 1.0. This result shows the good damage identification accuracy of damaged and undamaged cells. Compared with the finite element method, the most remarkable benefit of this approach is its ability to enhance computational efficiency. For a 10-cell continuous beam, the transfer method of the cell involves only a 4×4 matrix. If the finite element method is used, there will be 60 DOFs, and the dimensions of the global stiffness matrix will be 60×60. If the mesh density in the finite element method is higher, the computational workload will be considerably greater than that of the SEM. The iterative process of the objective function takes more computational resources. More time and computing resources can be saved for large-scale engineering.

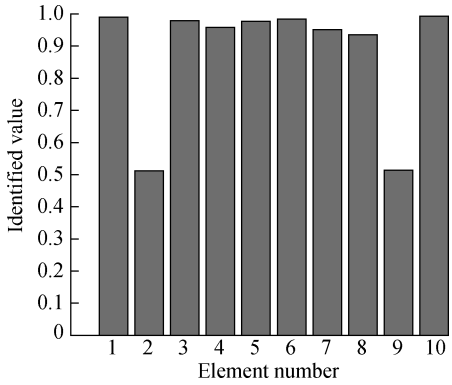

Fig. 8 Identified results of iterations for Case 5 in the numerical study

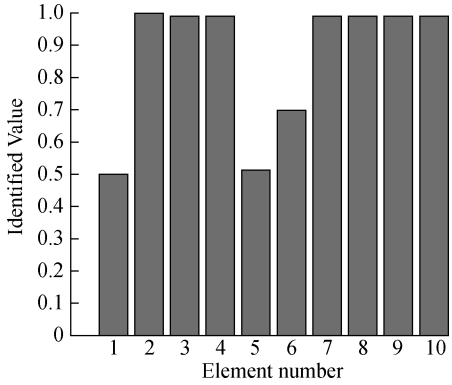

Fig. 9 Identified results of iterations for Case 6 in the numerical study

4 Conclusions

1) The dynamic stiffness matrix of an Euler beam in one cell is established using the SEM, and the equilibrium equation of a joint is obtained from the boundary continuity condition. By combining the dynamic stiffness matrix and equilibrium equation of a joint, the transfer matrix for the periodic continuous beam can be obtained.

2) The real part of the propagation constant is introduced to measure the degree of detuning. As the joint vertical stiffness of the cell increases, the number of stop bands remains constant. The width of the stop bands con-

sistently increases. In each frequency stop band, the lower limit of the range remains constant while the upper limit increases rapidly.

3) A damage identification method for identifying joint vertical stiffness in periodic continuous beams based on the SEM is proposed. The objective function of the damage identification method is based on the propagation constant.

4) The proposed method is extensively evaluated through numerical case studies. The results demonstrate its effectiveness in identifying single- and multi-parameter damage cases. The proposed damage identification method based on the propagation constant has good computational efficiency and accuracy.

5) The position and width of wave propagation band gaps determined by the propagation constant are validated by analyzing the transfer properties and deformation of periodic beams. The good qualitative agreement between transfer properties and band gap results obtained from the transfer matrix method verifies the correctness of the transfer matrix method and the presence of band gaps.

References

[1] Tu Y M, Lu S L, Wang C, Damage identification of steel truss bridges based on deep belief network [J]. *Journal of Southeast University* (*English Edition*), 2022, **38**(4): 392 − 400. DOI: 10.3969/j. issn. 1003-7985. 2022.04.008.

[2] Jiao H C, Yan Y D, Jin H. Evaluation of mechanical properties of cast steel nodes based on GTN damage model[J]. *Journal of Southeast University* (*English Edition*), 2021, **37**(4): 401 − 407. DOI: 10.3969/j. issn. 1003-7985.2021.04.009.

[3] Cawley P, Adams R D. The location of defects in structures from measurements of natural frequencies[J]. *The Journal of Strain Analysis for Engineering Design*, 1979, **14**(2): 49 − 57. DOI: 10.1243/03093247V142049.

[4] Wahab M M A, Roeck G D. Damage detection in bridges using modal curvatures: Application to a real damage scenario[J]. *Journal of Sound & Vibration*, 1999, **226**(2): 217 − 235. DOI: 10.1006/jsvi.1999.2295.

[5] Droz C, Boukadia R, Desmet W. A multi-scale model order reduction scheme for transient modelling of periodic structures[J]. *Journal of Sound and Vibration*, 2021, **510**: 116312. DOI: 10.1016/j. jsv.2021.116312.

[6] Duong H N, Magd A W. Damage detection in slab structures based on two-dimensional curvature[J]. *Advances in Engineering Software*, 2023, **176**: 103371. DOI: 10.1016/j. advengsoft.2022.103371.

[7] Gu H S, Itoh Y. Aging behaviors of natural rubber in isolation bearings[J]. *Advanced Materials Research*, 2010, **163**: 3343 − 3347. DOI: 10.4028/www. scientific. net/AMR.163-167.3343.

[8] Ying Z G, Ni Y Q, Dynamic characteristics of infinite-length and finite-length rods with high-wave-number periodic parameters[J]. *Journal of Sound & Vibration*, 2017, **24** (11): 2344 − 2358. DOI: 10.1177/1077546316687676.

[9] Hussein M I, Leamy M J, Ruzzene M, et al. Dynamics of phononic materials and structures: Historical origins, recent progress, and future outlook[J]. *Applied Mechanics Reviews,* 2014, **66**(4): 040802. DOI: 10.1115/1.4026911.

[10] Wei J, Petyt M. A method of analyzing finite periodic structures, part 2: Comparison with infinite periodic structure theory[J]. *Journal of Sound & Vibration*, 1997, **202**(4): 571 − 583. DOI: 10.1006/JSVI.1996.0888.

[11] Michaels T C T, Kusters R, Dear A J, et al. Geometric localization in supported elastic struts[J]. *Proceedings of the Royal Society A*, 2019, **475**(2229): 20190370. DOI: 10.1098/rspa.2019.0370.

[12] Bendiksen O O. Localization phenomena in structural dynamics[J]. *Chaos Solitons Fractals,* 2000, **11**(10): 1621 − 1660. DOI: 10.1016/S0960-0779(00)00013-8.

[13] Wierzbicki E, Woźniak C. On the dynamics of combined plane periodic structures[J]. *Archive of Applied Mechanics,* 2000, **70** (6): 387 − 398. DOI: 10.1007/S004199900070.

[14] Michalak B. Vibrations of plates with initial geometrical periodical imperfections interacting with a periodic elastic foundation[J]. *Archive of Applied Mechanics*, 2000, **70** (7): 508 − 518. DOI: 10.1007/S004190000081.

[15] Romeo F, Luongo A. Vibration reduction in piecewise bi-coupled periodic structures[J]. *Journal of Sound & Vibration,* 2003, **268**(3): 601 − 615. DOI: 10.1016/S0022-460X(03)00375-4.

[16] Hull A J. Dynamic response of an elastic plate containing periodic masses[J]. *Journal of Sound & Vibration*, 2008, **310**(1/2): 1 − 20. DOI: 10.1016/j. jsv.2007.03.085.

[17] Manktelow K L, Leamy M J, Ruzzene M. Analysis and experimental estimation of nonlinear dispersion in a periodic string[J]. *Journal of Vibration and Acoustics*: *Transactions of the ASME*. 2014, **136**(3): 031016. DOI: 10.1115/1.4027137/380275.

[18] Hvatov A, Sorokin S. Free vibrations of finite periodic structures in pass- and stop-bands of the counterpart infinite waveguides[J]. *Journal of Sound & Vibration,* 2015, **347**: 200 − 217. DOI: 10.1016/j. jsv.2015.03.003.

[19] Junyi L, Balint D S. An inverse method to determine the dispersion curves of periodic structures based on wave superposition[J]. *Journal of Sound & Vibration,* 2015, **350**: 41 − 72. DOI: 10.1016/j. jsv.2015.03.041.

[20] Wu Z J, Li F M. Spectral element method and its application in analysing the vibration band gap properties of two-dimensional square lattices[J]. *Journal of Vibration and Control*, 2014, **22** (3): 710 − 72. DOI: 10.1177/1077546314531805.

[21] Domadiya P G, Manconi E, Vanali M, et al. Numerical and experimental investigation of stopbands in finite and infinite periodic one-dimensional structures[J]. *Journal of Vibration and Control*, 2014, **22**(4): 920 − 931. DOI: 10.1177/1077546314537863.

[22] Chen J S, Tsai S M. Sandwich structures with periodic assemblies on elastic foundation under moving loads[J]. *Journal of Vibration and Control*, 2014, **22**(10): 2519 − 2529. DOI: 10.1177/1077546314548470.

[23] Ying Z G, Ni Y Q. A double expansion method for the

frequency response of finite-length beams with periodic parameters[J]. *Journal of Sound & Vibration,* 2017, **391**: 180 − 193. DOI: 10. 1016/J. JSV. 2016. 12. 011.

[24] Ying Z G, Ni Y Q. A response-adjustable sandwich beam with harmonic distribution parameters under stochastic excitations[J]. *International Journal of Structural Stability & Dynamics,* 2017, **17**: 1750075. DOI: 10. 1142/S0219455417500754.

[25] Heckl M A. Investigations on the vibrations of grillages and other simple beam structures[J]. *Journal of the acoustical Society of America,* 1964, **36**(7): 743 − 748. DOI: 10. 1121/1. 1919206.

[26] Mead D J. Free wave propagation in periodic supported, infinite beams[J]. *Journal of Sound & Vibration,* 1970, **11**: 181 − 197. DOI: 10. 1016/S0022-460X(70)80062-1.

[27] Mead D J. The forced vibration of one-dimensional multi-coupled periodic structures: An application to finite element analysis[J]. *Journal of Sound & Vibration,* 2009, **319**(1/2): 282 − 304. DOI: 10. 1016/J. JSV. 2008. 05. 026.

[28] Mead D J. Wave propagation in continuous periodic structures: Research contributions from southampton[J]. *Journal of Sound & Vibration,* 1996, **190**: 495 − 524. DOI: 10. 1006/JSVI. 1996. 0076.

[29] Mead D J, Parthan S. Free wave propagation in two-dimensional periodic plates[J]. *Journal of Sound & Vibration*, 1979, **64**: 325 − 348. DOI: 10. 1016/0022-460X(79)90581-9.

[30] Mead D J, Markuš S. Coupled flexural-longitudinal wave motion in a periodic beam[J]. *Journal of Sound & Vibration*, 1983, **90**: 1 − 24. DOI: 10. 1016/0022-460X(83)90399-1.

[31] Mukherjee S, Parthan S. Free wave propagation in rotationally restrained periodic plates[J]. *Journal of Sound & Vibration,* 1993, **163**: 535 − 544. DOI: 10. 1006/JSVI. 1993. 1186.

[32] Koo G H, Park Y S. Vibration reduction by using periodic supports in a piping system[J], *Journal of Sound & Vibration*, 1998, **210**(1): 53 − 68. DOI: 10. 1006/JSVI. 1997. 1292.

[33] Zhang S, Fan W. An exact spectral formulation for the wave characteristics in an infinite Timoshenko-Ehrenfest beam supported by periodic elastic foundations[J]. *Computers & Structures*, 2023, **286**: 107105. Doi. org/10. 1016/j. compstruc. 2023. 107105.

[34] Ying Z G, Ni Y Q, Kang L. Mode localization characteristics of damaged quasiperiodic supported beam structures with local weak coupling[J]. *Structural Control & Health Monitoring*, 2019, **26**(6): e2351. DOI: 10. 1002/stc. 2351.

[35] Pierre C. Mode localization and eigenvalue loci veering phenomena in disordered structures[J]. *Journal of Sound & Vibration*, 1988, **126**(3): 485 − 502. DOI: 10. 1016/0022-460X(88)90226-X.

[36] Zhao T, Yang Z, Xu Y, et al. Mode localization in metastructure with T-type resonators for broadband vibration suppression[J]. *Engineering Structures*, 2022, **268**: 114775. DOI: 10. 1016/0022-460X(88)90226-X.

基于谱元法的周期连续梁接头竖向刚度损伤识别

朱宏平　申泽辉　翁　顺

(华中科技大学土木与水利工程学院, 武汉 430074)

摘要: 为识别周期连续梁支承的损伤,提出了一种基于谱元法的周期连续梁接头竖向刚度损伤识别方法. 以周期欧拉梁为研究对象,每1个周期胞元由1个梁单元和2个梁单元间的接头组成,采用谱元法得到1个胞元内梁单元的动刚度矩阵,并结合接头平衡方程,建立周期连续梁的传递矩阵. 通过求解传递矩阵的特征值得到传播常数,进而建立基于传播常数的目标函数,利用内点法实现周期连续梁接头竖向刚度损伤识别. 数值算例结果表明,所提方法能够准确识别接头竖向刚度的损伤位置和损伤程度.

关键词: 接头;周期连续梁;波传播;谱元法;传播常数

中图分类号: TU352